Supplementary Data

Telomere Maintenance Mechanisms Define Clinical Outcome in High-Risk Neuroblastoma

Balakrishna Koneru,[1, 2] Gonzalo Lopez,[3, 4] Ahsan Farooqi,[1, 2] Karina L. Conkrite,[3,4] Thinh H. Nguyen,[1] Shawn J. Macha,[1, 2] Apexa Modi,[3, 4] Jo Lynne Rokita,[3,4,5] Eduardo Urias,[1] Ashly Hindle,[1,2] Heather Davidson,[1] Kristyn Mccoy,[1] Jonas Nance,[1] Vanda Yazdani,[1] Meredith S. Irwin,[7] Shengping Yang,[1] David A. Wheeler,[6] John M. Maris,[3] Sharon J. Diskin,[3, 4] C. Patrick Reynolds[1,2]

Author Affiliations

[1]Cancer Center and Department of Pediatrics, School of Medicine, Texas Tech University Health Sciences Center School of Medicine, Lubbock, TX, USA.

[2]Department of Cell Biology and Biochemistry, Texas Tech University Health Sciences Center, Lubbock, TX, USA.

[3]Division of Oncology, Children's Hospital of Philadelphia and Perelman School of Medicine at the University of Pennsylvania, Philadelphia, PA, 19104-4318, USA.

[4]Department of Bioinformatics and Health Informatics, Children's Hospital of Philadelphia, Philadelphia, PA, 19104, USA.

[5]Center for Data-Driven Discovery in Biomedicine, Children's Hospital of Philadelphia, Philadelphia, PA, 19104, USA.

[6]Human Genome Sequencing Center, Baylor College of Medicine, Houston, TX, 77030, USA.

[7]Department of Pediatrics, The Hospital for Sick Children, Toronto, ON, Canada

Table of Contents

Supplementary Tables

Materials and Methods:

Study Design

Telomere maintenance mechanisms (TMM) were studied using C-circle assay, telomere content assay, *TERT* mRNA expression (RNAseq), WGS/WES sequencing, and clinical covariates in 134 primary neuroblastoma tumors (110 high-, 12 intermediate- and 12- low-risk samples) selected solely based on the availability of RNAseq and DNA. We assessed telomere maintenance mechanisms in 103 patient-derived cell lines and 28 patient-derived xenografts (PDXs) established from high-risk neuroblastomas by the COG/ALSF Childhood Cancer Repository (www.CCcells.org), details are in supplementary methods. To reduce heterogeneity, we restricted our survival analysis to 107 high-risk neuroblastoma samples from stage 4 patients with age at diagnosis > 18 months. Median *TERT* mRNA expression was the cutoff to define TERT-high and TERT-low groups. Source of sequencing data is indicated in their respective sections.

Human Subjects:

All primary human specimens were obtained after written informed consent was obtained at Children's Oncology Group member institutions through NCI TARGET initiative (1). Patient derived neuroblastoma cell lines and PDXs were obtained from the COG/ALSF Childhood Cancer Repository (www.CCcells.org), which obtained informed consent at appropriate institutions before acquiring the patient material. All studies were conducted in accordance with recognized ethical guidelines.

Description of Patient Dataset and Source

The whole genome/exome- and RNA-sequencing datasets are available directly through NCBI dbGaP (https://www.ncbi.nlm.nih.gov/gap) with study-id phs000218 and accession number:

Neuroblastoma (NBL)-phs000467. WGS, WES and RNA-seq for patient samples were obtained by TARGET NCI initiative. Processed datasets and clinical covariates are available at the Therapeutically Applicable Research to Generate Effective Treatments (TARGET) initiative (https://ocg.cancer.gov/programs/target) data matrix. All samples were obtained through the Children's Oncology Group (COG). C-circle assay, telomere content assay and *TERT* mRNA expression (qPCR) analysis were performed in the investigators laboratory.

RNA Sequencing Analysis

RNA sequencing for 134 TARGET NBL patients were initially aligned using STAR using as reference all known transcripts from GENCODE. In addition, *de novo* transcripts were identified and quantified using StringTie (2), altogether resulting in the identification of 43 *ATRX* transcripts (8 previously reported in GENCODE and 35 novel transcripts). We classified transcripts according to their aberrant status into 'coding', 'non-coding', 'likely-coding', 'in-frame-fusions' and 'altered'. We then aggregated the expression of all coding transcripts and compared against the aggregated expression of all in-frame-fusion transcripts in order to identify samples overexpressing only the aberrant isoforms (Fig. S2).

***TERT* Expression Threshold**

Median *TERT* mRNA expression of the high-risk (age>18 months; n=107) cohort was used to define *TERT*-high (TERT-H) and *TERT*-low (TERT-L) groups for an unbiased clinical classification. We also identified a *TERT* expression threshold for RNAseq data to differentiate *TERT* positive and *TERT* negative tumors, similar to an approach used for TERT RNA microarray data (3), by fitting a mixture of two normal distributions using expectation maximization algorithm (mixtools package in R). Tumors having a posterior probability of

>95% for the second component were considered as *TERT* positive and reminder were classified as *TERT* negative.

Sanger Sequence Validation

For validation of *ATRX* wild-type ALT tumors, Sanger sequencing was performed as described previously (3).

Neuroblastoma Cell Lines and Patient-Derived Xenografts

All neuroblastoma patient-derived cell lines and patient-derived xenografts (PDXs) were obtained from the ALSF/Children's Oncology Group (COG) Childhood Cancer Repository at the Texas Tech University Health Sciences Center (www.CCcells.org). COG- and CHLA- cell lines were cultured in Iscove's Modified Dulbecco's Medium supplemented with 1 X ITS, 4 mM L-glutamine, and 20% fetal bovine serum (FBS) (GIBCO) or with serum free neurobasal media supplemented with EGF, FGF, B-27 and N-2 supplements in cell lines where their name is followed by hnb and nb. SMS-, SK-N- and LA-N- series of cell lines were grown in RPMI-1640 supplemented with 10% FBS. Cell lines with h as suffix are grown in 5% O2, and with h2 are grown in 2% O2. Cell line identities were confirmed using the AmpFLSTR Identifier Plus PCR Amplification kit (Applied Biosystems) at time of use for experimentation, verified against the STR database at www.CCCells.org and were routinely tested for lack of mycoplasma contamination. Neuroblastoma cell lines were used at passage numbers below 25, except when noted in results. HEK293FT cells (ThemoFischer Scientific) were cultured in DMEM supplemented with tetracycline-free 10% FBS, 4 mM L-glutamine, 1 mM MEM sodium pyruvate and 1% Pen-Strep (GIBCO). Cell viability was measured using a Beckman Coulter Vi-CELL.

A total of 28 PDXs were used in this study all employed at passage 2 in mice. All PDX identities were confirmed using the AmpFLSTR Identifier Plus PCR Amplification kit (Applied Biosystems) at time of use for experimentation, verified against the STR database at www.CCCells.org. PDXs were all verified to be free of human pathogens and Epstein-Barr virus by PCR. All animal studies were approved by the Texas Tech University Health Sciences Center Institutional Animal Care and Use Committee. Six- to 8-week-old athymic (nu/nu) mice (Jackson Laboratory) were injected subcutaneously with 10 million PDX cells (previously passed at least once in nu/nu mice). The tumor volume and mouse weights were measured at least once weekly. Tumor volumes were calculated as 0.5*height * width * length (4). The event-free survival (EFS) time was defined as the time required for the tumor to grow from 150-250mm^3 to the endpoint (tumor volume $\geq$ 1500 mm^3), as described previously (5). Tissue obtained at the endpoint was verified for identity by STR profiling (www.CCcells.org). Sequencing data for PDXs can be obtained at dbGAP under accession number phs001437 (6).

ATRX and MYCN Knockdown

Lentiviral particles encoding control eGFP shRNA (SHC005, sigma) and 2 hairpins each against *MYCN* (TRCN0000020694, TRCN0000020695) and *ATRX* (TRCN0000013590, TRCN0000013592) were purchased from sigma. Neuroblastoma cell lines were transduced with lentiviral particles encoding shRNA in the presence of 4-8 μg/ml hexadimethrine bromide for 48 hours. Following transduction, selection with 1.5 μg/ml puromycin (Sigma) was initiated. *MYCN* or *ATRX* mRNA knockdown and protein knockdown were confirmed by qPCR and by immunoblotting, respectively.

Immunoblotting

Whole cell lysates were prepared with RIPA buffer (Thermo Fisher) supplemented with 1 X

Protease/Phosphatase Inhibitor Cocktail (Cell Signaling Technology), briefly sonicated, vortexed for 15 minutes at 4°C, and then centrifuged for 30 minutes. Supernatant containing the protein was isolated and quantified using BCA assay. A total of 25 µg of protein lysate was separated on 4-12% Bis-Tris gels using MOPS (Life Technologies) running buffer, transferred on to a 0.45 µm PVDF membrane (GE Healthcare Life Sciences), blocked with 5% bovine serum albumin (BSA) in Tris-buffered saline and 0.1% Tween-20 (TBST). The membranes were incubated overnight with primary antibody at 4°C, washed 3X for 5 minutes with TBST, incubated in 1:1000 diluted HRP-conjugated secondary antibody (Cell Signaling Technology) for 1 hour at room temperature, washed 3X for 5 minutes with TBST, and developed with Amersham ECL Western Blotting Detection Reagent (GE Healthcare Life Sciences). Primary antibodies used in this study were β-Actin (1:5000; #sc-47778, Santa Cruz Biotechnology), ATRX (1:1000; #sc-55584, Santa Cruz Biotechnology), DAXX (1:1000; sc-8043, Santa Cruz Biotechnology), and MYCN (1:1000; #9405S, Cell Signaling Technology).

Immunohistochemistry (IHC)

Immunohistochemical staining was performed on 4 µm unstained sections from formalin-fixed paraffin-embedded (FFPE) tissue blocks for each neuroblastoma PDX. Slides were first deparaffinized with serial xylene treatment for 5 minutes each, followed by hydration in a graded ethanol series. The hydrated slide sections were steamed for 45 minutes with EDTA buffer (pH 9.0) for anti-ATRX and citrate buffer (pH 6.0) for anti-DAXX. After slides were cooled down at RT for 10 minutes, sections were blocked with Dual Endogenous Enzyme-Blocking Agent (Dako) for 10 minutes. Sections were incubated with either anti-ATRX (1:400, #HPA001906, Sigma-Aldrich) or anti-DAXX (1:50, #HPA008736, Sigma-Aldrich) for 1 hour, followed by anti-rabbit secondary antibody (Leica Microsystems) for 30 minutes at room temperature, and

detected with 3, 3'-diaminobenzidine (Sigma-Aldrich). All wash steps were performed with PBS containing 0.1% Tween-20 three times for 5 minutes. Finally, sections were counterstained with hematoxylin, dehydrated with a graded ethanol and xylene series, and were mounted for microscopy. A minimum of 3 sections and 3 images per section were captured per PDX. Sections were considered positive for ATRX and DAXX if greater than 5% of cancer cells had positive nuclear staining as described previously (3). Sections were considered negative for nuclear staining if nuclear labeling of adjacent mouse lymphocytes was present.

C-circle Assay and Telomere qPCR

C-circles in whole genomic DNA were amplified by rolling circle amplification using Φ29 polymerase as described previously (7-9). Each sample reaction was performed with or without Φ29 DNA polymerase; 20 µl C-circle assay reaction contained 1 x Φ29 DNA polymerase buffer, 1 mM dATP, 1 mM dCTP, 1 mM dGTP, 1 mM dTTP, 0.1% Tween-20, and 4 µM DTT, with or without Φ29 polymerase (NEB). C-circle assay products were detected by qPCR or slot blotting.

For detection of C-circle assay products by qPCR, 20 µL of C-circle assay product was diluted with 20 µL of TE buffer, and 5 µL of the diluted C-circle assay product was used for each of 6 PCR reactions: Telomere qPCR of C-circle assay reaction with Φ29 DNA polymerase in triplicates, telomere PCR of C-circle assay reaction without Φ29 DNA polymerase in triplicate, single copy gene (SCG) PCR of C-circle assay reaction with Φ29 DNA polymerase in triplicate, and SCG PCR of C-circle assay reaction without Φ29 DNA polymerase. VAV2 was used as the single copy gene for all neuroblastoma patient tumors, PDXs, and cell lines as reported previously (9). Each 25 µL qPCR reaction consisted of 1X QuantiTect SYBR Green PCR Master Mix (Qiagen), 5 µL DNA template, and primer sets. The final primer concentrations were 400 nM telomere forward, 900 nM telomere reverse, 200 nM VAV2 forward, and 200 nM

VAV2 reverse. All the PCR reactions were performed with a CFX96 real-time PCR system (Bio-Rad). PCR conditions were: Tel: 95°C for 15 min, 33 cycles of 95°C for 15 sec and 56°C for 2 min, and VAV2: 95°C for 15 min, 40 cycles of 95°C for 15 sec, 57°C for 30 sec, and 72°C for 1 min. Telomere product was normalized to the SCG product. All PCR results were expressed as mean of triplicate reactions. The relative total telomeric DNA content (TC) of a sample was the normal TC obtained from the C-circle assay without Φ29 and was relative to the TC of the ALT-positive cell line CHLA-90 defined as having a value of 5.0. The relative C-circle level of a sample was calculated: [normalized telomere content with Φ29] – [normalized telomere content without Φ29] and was expressed relative to the C-circle level of CHLA-90 defined as having a value of 100. Consistent with previous studies (10), a sample was considered C-circle positive if the C-circle level was ≥5. Neuroblastoma cell line CHLA-20 (telomerase-positive) was used as a negative control.

To detect C-circles by slot-blot analysis, a 20 µL C-circle assay product was diluted with 100 µL of 2X saline sodium citrate buffer (SSC) and slot-blotted onto a positively charged nylon membrane (Roche) using Minifold II Slot-Blot Manifold (Cole-Parmer). The membrane was UV-cross-linked, and hybridized using DIG labeling probe $(CCCTAA)_4$, as described previously (11). The membrane was imaged on VersaDoc Imaging System (Bio-Rad) for chemiluminescence with cutoffs as described above for determining C-circle positivity.

Terminal Restriction Fragment (TRF) Analysis

Whole genomic DNA was digested with RsaI and HinfI restriction enzymes, and resolved on a 0.8% agarose gel using either conventional agarose electrophoresis or pulse-field gel electrophoresis. Separated DNA fragments were detected with *TeloTAGGG* telomere length assay kit (Roche).

Telomere Abundance and Telomere Ratio from Whole Genome Sequencing Data

In order to process CGI data we first downloaded sequences from the sequence read archive (SRA) using fastdump (attribute –f special) tool included in sra-toolkit (v2.8.0). CGI uses sequencing by probe-anchor ligation technology (12) which produce short read pairs (35bp each) from fragments ~500 bp length from the same strand. The sequence reads incorporate gaps following a non-random distribution. Provided the short read length and gapped structure as well as the unavailability of aligners for this technology, it was not feasible to align telomeric repeat sequences in order to estimate telomere length, as Illumina based methods do. We quantified the amount of telomeric DNA in each sample by obtaining the number of telomeric reads per million reads. Our custom telomere counter script counts the number of canonical telomere repeats (TTAGGG/CCCTAA) in each read, defining telomeric reads as those containing at least 3 repeats in each pair.

ALT Classification via Detection of APBs in Patient Tumor Tissue.

APB staining on formalin fixed paraffin embedded (FFPE) sections was performed as described previously (13). A strict criteria was used to determine the APB status in a tumor sections, as described previously (3,14,15). An APB was considered to be present if positive staining for telomeric DNA was localized within a PML body in the nucleus. To avoid false positive detection of APBs, the telomeric DNA in the APB should have a more intense fluorescence than that of the telomeres in the same tissue section (the working criterion we used with the FITC-labeled telomeric probe was to require that with the appropriate camera exposure for the telomeric DNA in the APB, the telomeres were barely visible). The sections were scored as positive for APBs if they were detected in ≥5 and in ≥0.5% of the cells in the section. Slides were not scored as negative

unless >1000 tumor cells in 2 separate sections were examined. Images were obtained with a Nikon Ti-E microscope with an A1 confocal system. Fiji software was used for image analysis.

Telomere and Centromere FISH

FFPE sections (4 μm) were deparaffinized using xylene, hydrated through a graded ethanol series, washed in ddH_2O with 1% Tween-20, followed by heat-induced antigen retrieval for 30 minutes in citrate buffer (pH 6.0), then rinsed in ddH_2O and dehydrated in a graded ethanol series. Slides were incubated for 5 minutes at 80°C with TelC-Cy3, a telomere probe (PNA Bio) and CENT-FAM, a human-specific Pan-centromere probe (PNA Bio) diluted in hybridization solution. Hybridization was continued overnight in a humidified chamber. Slides were washed twice for 15 minutes each with hybridization wash buffer 1 (10 mM Tris-HCl pH 7.2, 70% deionized formamide, and 0.1% BSA) and 3 times for 5 minutes each with hybridization wash buffer 2 (0.1 M Tris-HCl pH 7.2, 0.15 M NaCl, 0.08% Tween-20). Slides were dehydrated in a graded ethanol series at RT and air dried. Slides were mounted with ProLong antifade Gold with DAPI (Invitrogen). The telomere/centromere fluorescence intensity was obtained by analyzing a minimum of 50 individual cells per PDX.

In the case of telomere FISH on metaphase spreads, cell cultures were treated with 1 μg/ml colcemid for 1-4 hours, followed by incubation in a hypotonic solution for 10 min at 37°C. The cells were fixed with 3:1 ice-cold methanol:acetic acid overnight at -20°C. The following day the cells were dropped onto SuperFrost Plus glass slides. Telomere FISH was performed on these slides as described above with TelC-Cy3 probe. Images were obtained with a Nikon Ti-E microscope with A1 confocal system. Representative 2D images in the figures are maximum intensity projections of the Z stack. Images were analyzed using Fiji software.

Real Time qPCR, and *MYCN* Copy Number Assay

RNA from cell lines and PDXs was extracted using a RNeasy Mini Kit (Qiagen), reverse transcription to cDNA was performed using a High Capacity cDNA Reverse Transcription Kit (Applied Biosystems). *TERT*, *TERC*, *MYCN*, and *GAPDH* expression were quantified using TaqMan Gene Expression Master Mix (Applied Biosystems) and TaqMan Gene Expression Assay primer probe sets (Applied Biosystems). Telomerase-positive cell line LA-N-5 was used to obtain relative *TERT* expression. *TERT* mRNA expression for all neuroblastoma cell lines and PDXs was normalized to *TERT* mRNA of LA-N-5 arbitrarily defined as a value of 5000. *MYCN* copy number for neuroblastoma cell lines and PDXs was determined using TaqMan copy number assay, using *MYCN* copy number probe (#4400291, Applied Biosystems), and RNAseP (#4403328, Applied Biosystems) as single copy reference gene (16). Neuroblastoma cell lines and PDXs with *MYCN* copy number >10 were designated as *MYCN*-amplified.

Supplementary Figures.

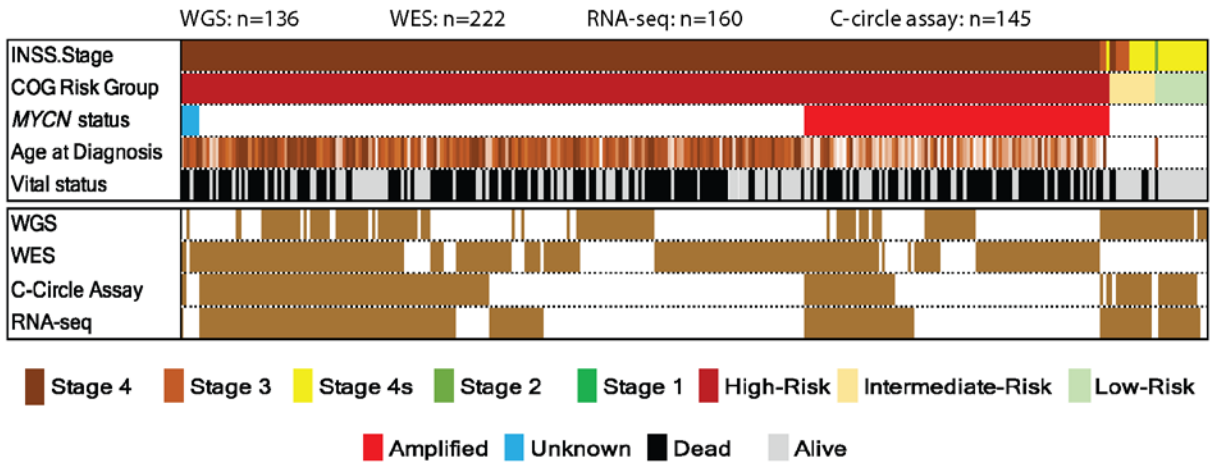

Fig. S1. Summary of clinical, genomic, and transcriptomic data available through the NCI TARGET initiative along with c-circle assay obtained as a part of this study. Data tracks clinical assessment (INSS stage, risk, *MYCN* status, age at diagnosis, and vital status), available genomic data sets (WGS and WES), and RNA sequencing across 316 neuroblastoma samples through TARGET initiative. C-circle assay (n=145) acquired as a part of this study was also included.

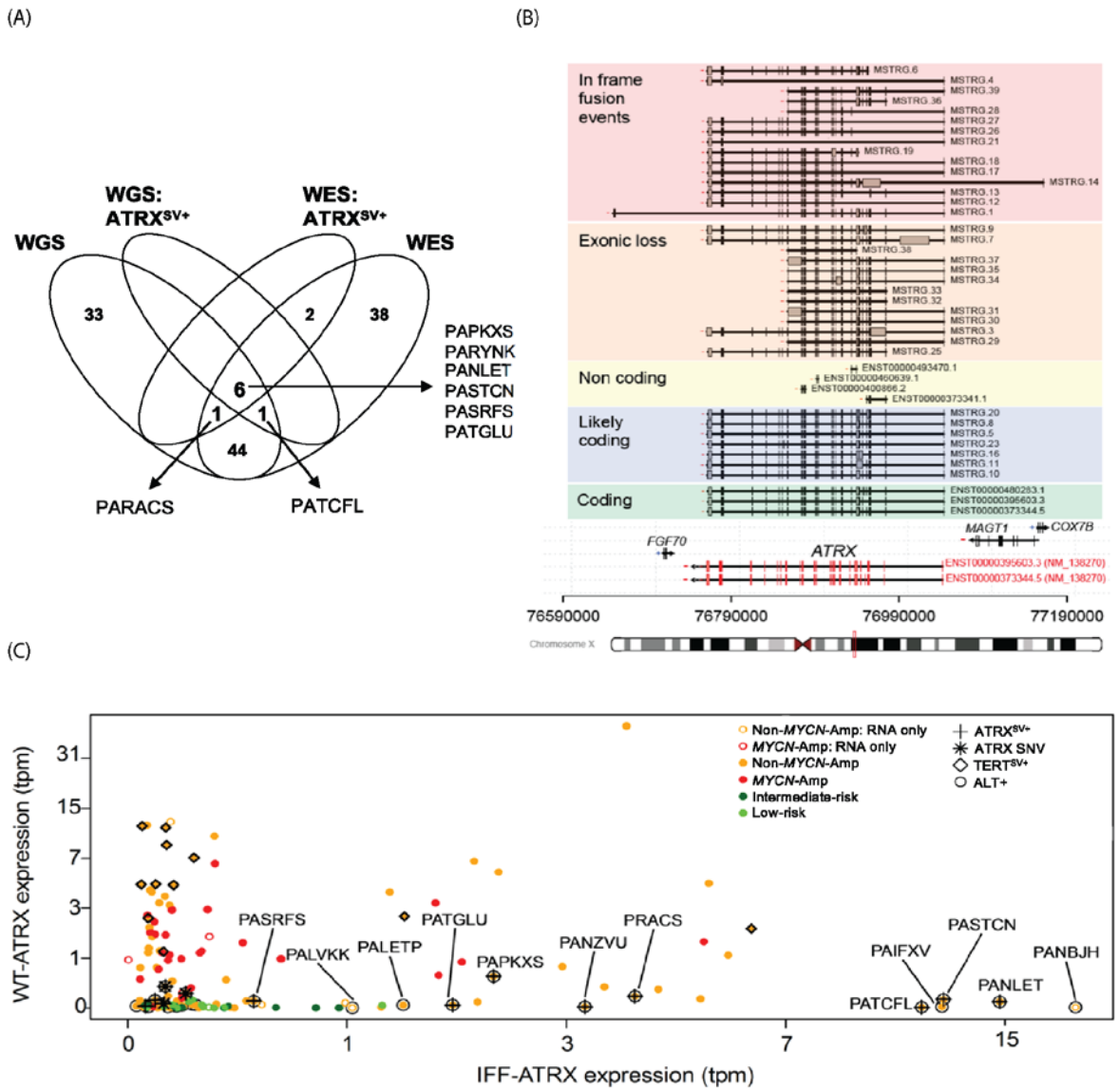

Fig. S2. *ATRX* variant validation and aberrant isoform in neuroblastoma subtypes. (A) Figure describes *ATRX* structural variant detected by WES and WGS studies that overlapped with c-circle assay and RNA-seq, 6 cased were detected by both WES and WGS; 1 *ATRX* SV is missed by the WGS and 1 was missed by WES. (B) StringTie *de novo* assembled transcripts using all TARGET RNA-seq neuroblastoma samples predicts known transcripts as well as novel aberrant isoforms. (C) Scatter plot comparing IFF-*ATRX* expression versus coding and likely *ATRX* isoforms across 134 neuroblastomas with RNA-seq and C-circle data; *ATRX*, *TERT* genetic status, *MYCN* amplification, risk category and C-circle (ALT) positivity are represented in combination of unique symbols and solid colors.

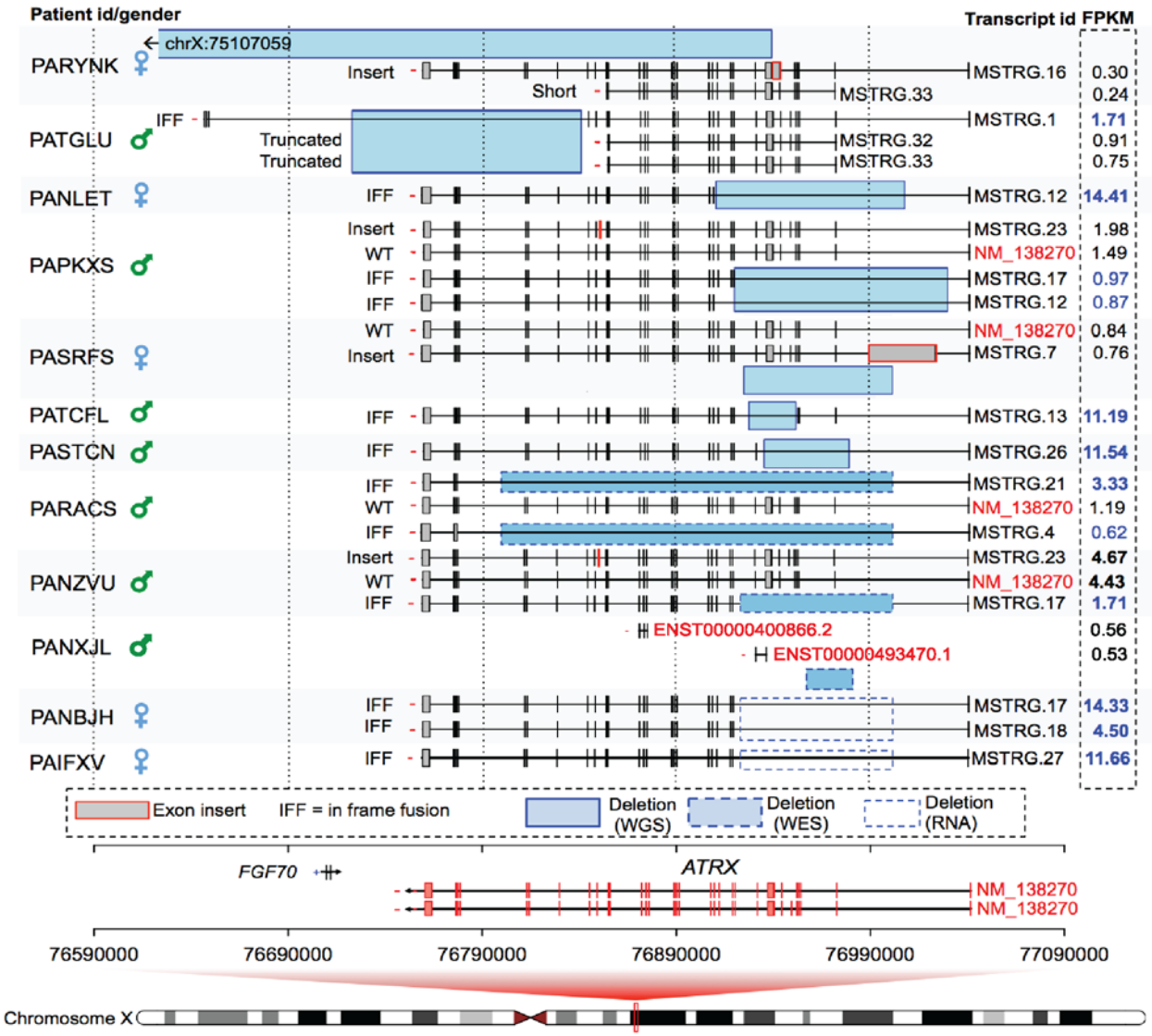

Fig. S3. ATRX variants detected in ALT tumors. Genomic track view representation of the *ATRX* gene locus shows multiple intragenic deletions and a tandem duplication overlaid with *de novo* transcript quantification from RNA-seq in ALT tumors. Novel transcripts represent intragenic in-frame fusion (IFF) events.

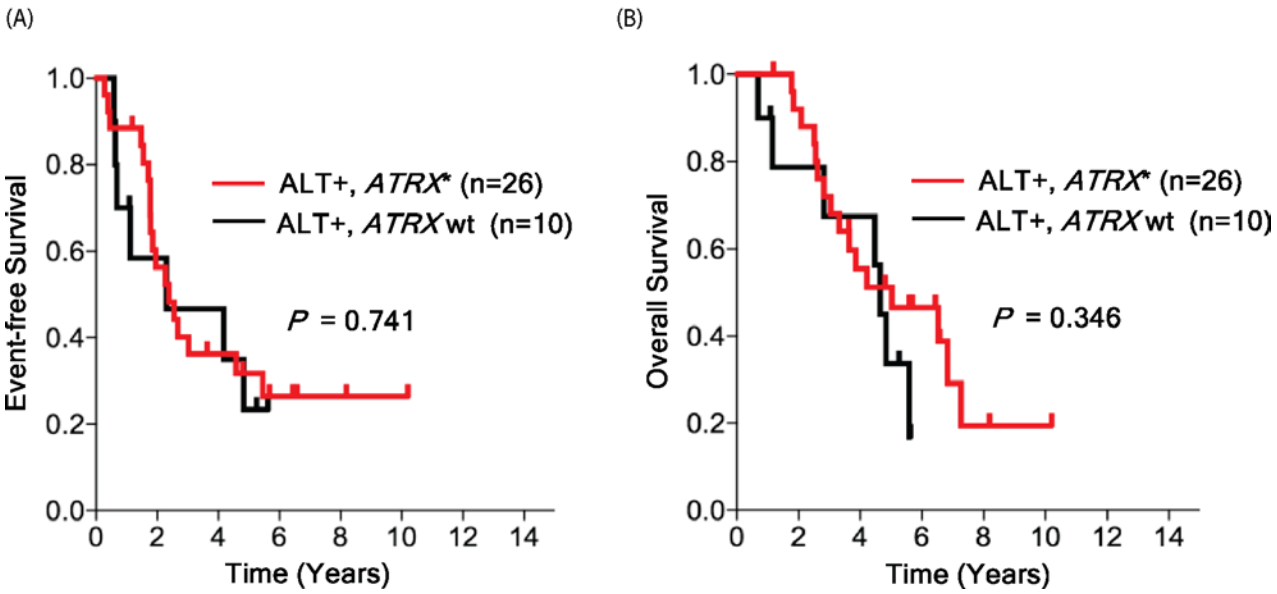

Fig. S4. Outcomes in ALT patients based on *ATRX* status. (A) Event-free survival (EFS) in ALT patients segregated by *ATRX* genomic alterations. ALT patients with *ATRX* genomic alterations (*ATRX**) are represented in red. ALT patients with *ATRX* wild-type (*ATRX* wt) are represented in black. (B) Overall survival (OS) in same groups as A. *P*-value was calculated using the log-rank test

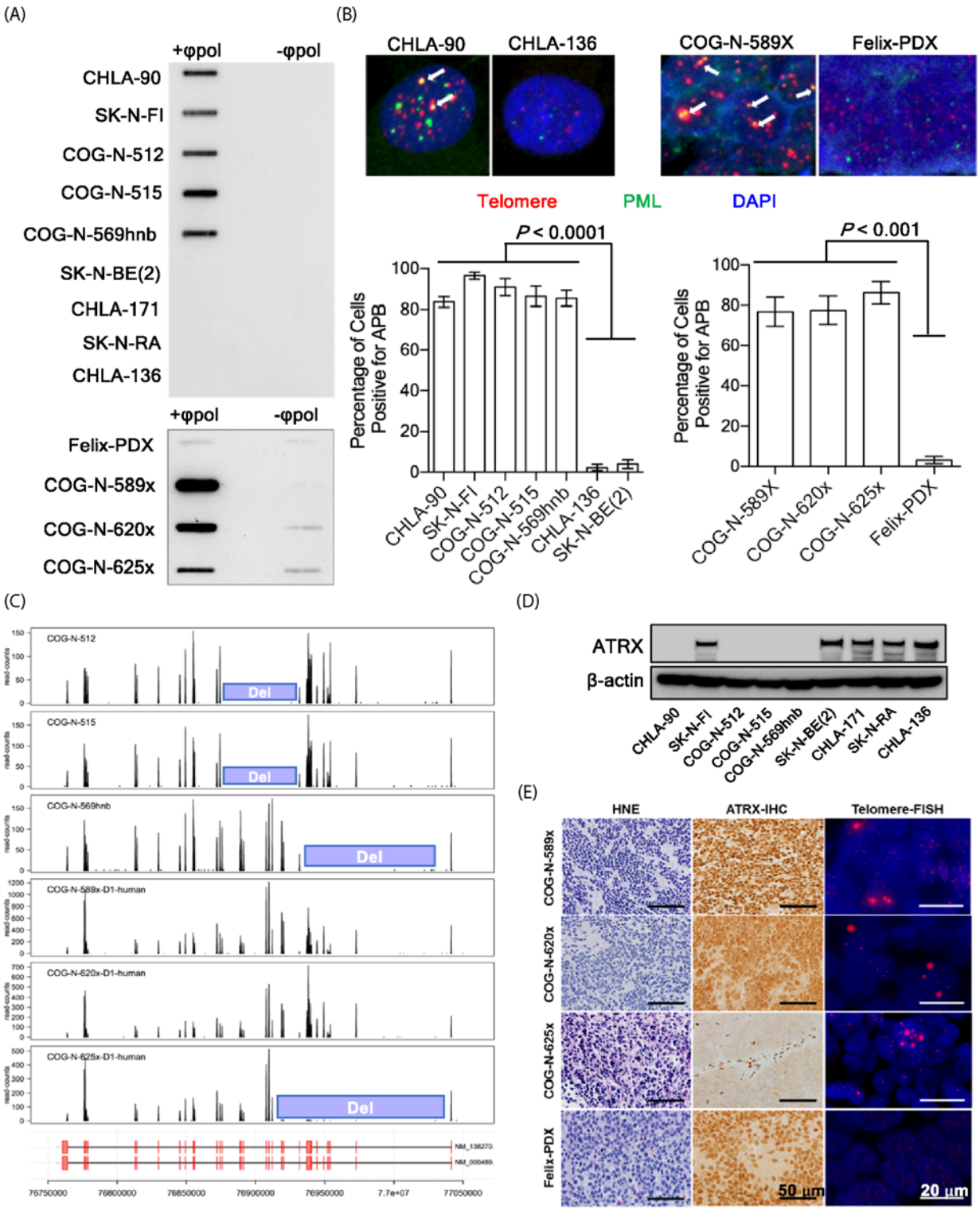

Fig. S5. ***ATRX*** **deletions and ATRX protein expression in ALT neuroblastoma cell lines and patient-derived xenografts.** (A) Confirmatory C-circle assay by slot blotting in 5 ALT neuroblastoma cell lines (CHLA-90, SK-N-FI, COG-N-512, COG-N-515, COG-N-569hnb) and 3 ALT patient-derived xenografts (PDXs; COG-N-589x, COG-N-620x and COG-N-625x) that were

initially identified as ALT models by qPCR. Telomerase-positive cell lines (SK-N-BE(2), CHLA-171, SK-N-RA, and CHLA-136) and PDX (Felix-PDX) were included for comparison. (B) Representative images of APB analysis by IF-FISH (top panel) in ALT (CHLA-90 and COG-N-589x) and telomerase-positive (CHLA-136 and Felix-PDX) models. Telomeres are shown in red, PML bodies in green, and nuclei with DAPI. Bar graph represents percentage of APB-positive cells (bottom panels) in ALT (CHLA-90, SK-N-FI, COG-N-512, COG-N-515, COG-N-569hnb, COG-N-589x, COG-N-620x, and COG-N-625x) compared to telomerase-positive models (CHLA-136, SK-N-BE(2), and Felix-PDX). (C) Graph shows exon read counts at *ATRX* locus. Location of predicted focal deletions at *ATRX* loci in COG-N-515, COG-N-512, COG-N-569hnb and COG-N-625x are represented in blue. (D) Immunoblot for ATRX and β-actin in same cell lines as A. (E) H&E staining, ATRX immunohistochemistry and telomere FISH on ALT PDXs (COG-N-589x, COG-N-620x and COG-N-625x) compared to a telomerase-positive PDX (Felix-PDX).

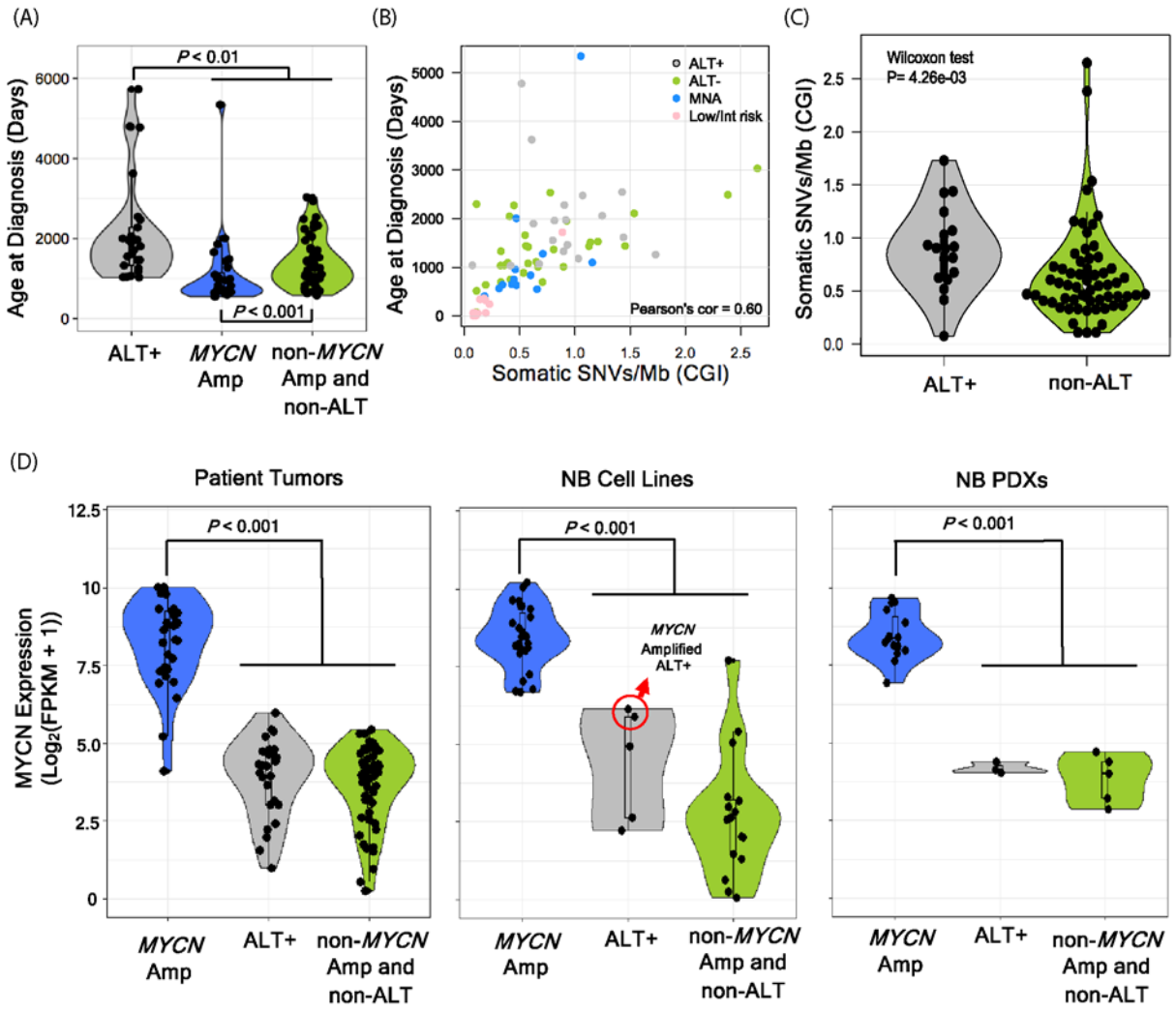

Fig. S6. ALT neuroblastoma is associated with higher age, higher mutation burden and low *MYCN* mRNA expression. (A) Age at diagnosis in high-risk NB patients (n=110), based on *MYCN* amplification and ALT status. (B) Correlation of somatic CGI burden determined by WGS versus age at diagnosis. (C) Box-plot showing comparison of somatic CGI burden based on ALT status in high-risk neuroblastoma patients with WGS data. (D) MYCN expression measured by RNA-seq in neuroblastoma primary patient tumors, cell lines, and patient derived xenografts based on *MYCN* amplification and ALT status. The 2 ALT cell lines that have *MYCN* amplification by copy number assay are circled in red. **. $P < 0.01$, ***: P<0.001; ****: P < 0.0001. *P*-value was calculated using Wilcoxon sum rank test.

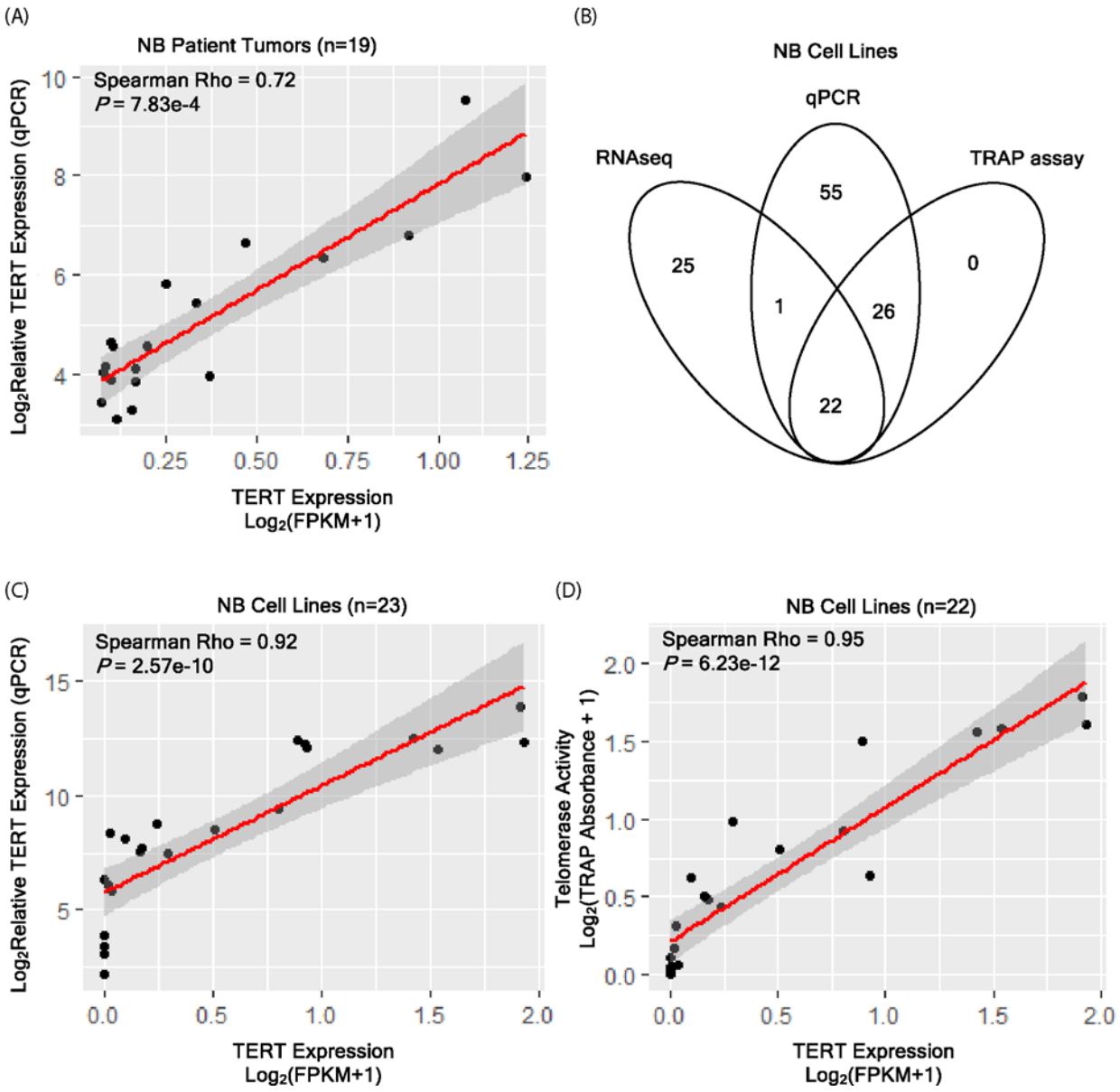

Fig. S7. Correlation of telomerase activity and TERT expression in neuroblastoma. (A) Spearman correlation of *TERT* mRNA expression measured by qPCR versus RNA-seq in primary patient tumors. (B) RNA-seq, *TERT* mRNA expression by qPCR, and TRAP assay data availability and overlap in neuroblastoma cell lines. (C) Correlation of *TERT* mRNA expression measured by qPCR versus RNA-seq in neuroblastoma cell lines. (D) Correlation of telomerase activity versus *TERT* expression by RNA-seq in neuroblastoma cell lines. Correlation was determined using spearman correlation test.

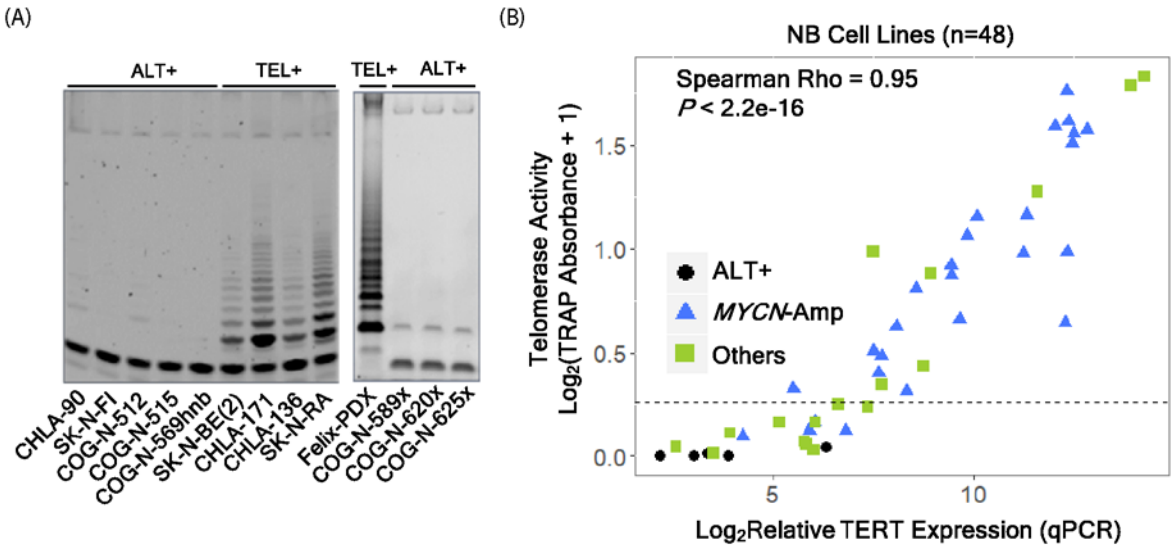

Fig. S8. TERT expression and telomerase activity in neuroblastoma cell lines and PDXs based on ALT status and *MYCN* amplification. (A) TRAP assay in ALT cell lines (CHLA-90, SK-N-FI, COG-N-512, COG-N-515, COG-N-569hnb) and patient-derived xenografts (COG-N-589x, COG-N-620x and COG-N-625x). Telomerase activated models are shown for comparison (SK-N-BE(2), CHLA-171, SK-N-RA, CHLA-136, and Felix-PDX). (B) Correlation of telomerase activity determined by TRAP PCR ELISA versus relative *TERT* expression by qPCR in 48 neuroblastoma cell lines based on ALT status and *MYCN* amplification. Correlation was determined using spearman correlation test.

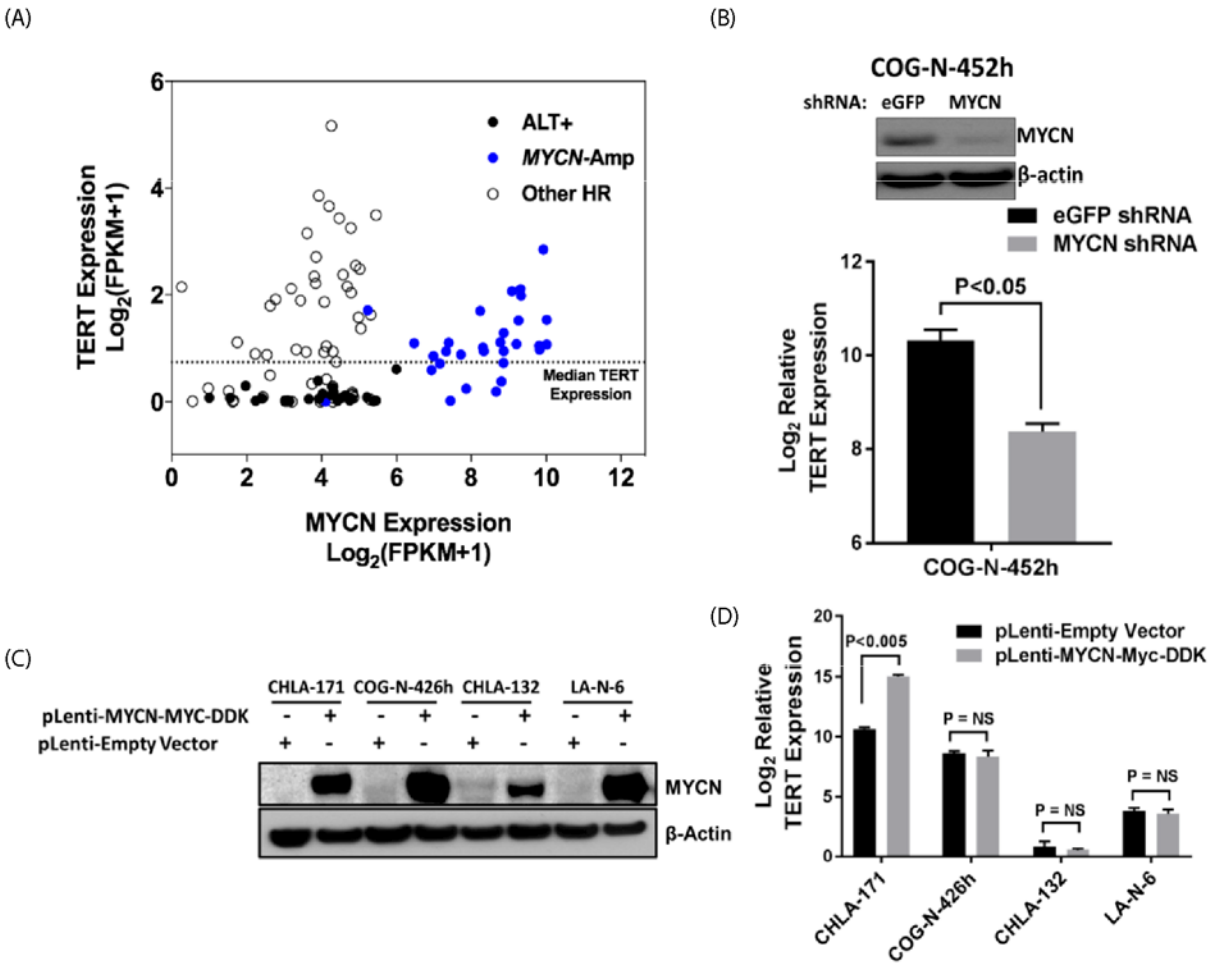

Fig. S9. Changes in *TERT* mRNA expression upon depletion and overexpression of *MYCN*. (A) Dot plot of *TERT* versus *MYCN* mRNA expression as measured by RNA-seq in 110 high-risk neuroblastoma patients. *MYCN*-amplified tumors are highlighted in blue and ALT patients are shown in black. The y-intercept represents median *TERT* expression cutoff of high-risk cohort. (B) Immunoblot (top panel) representing knockdown of MYCN in *MYCN*-amplified neuroblastoma cell line COG-N-452h. Bar graph (bottom panel) shows relative *TERT* expression following MYCN knockdown. (C) Immunoblot showing overexpression of MYCN in 4 non-*MYCN*-Amp neuroblastoma cell lines (D) Bar graph showing relative *TERT* expression following MYCN overexpression in the same neuroblastoma cell lines as shown in C. *P*-value was determined using two tailed t-test.

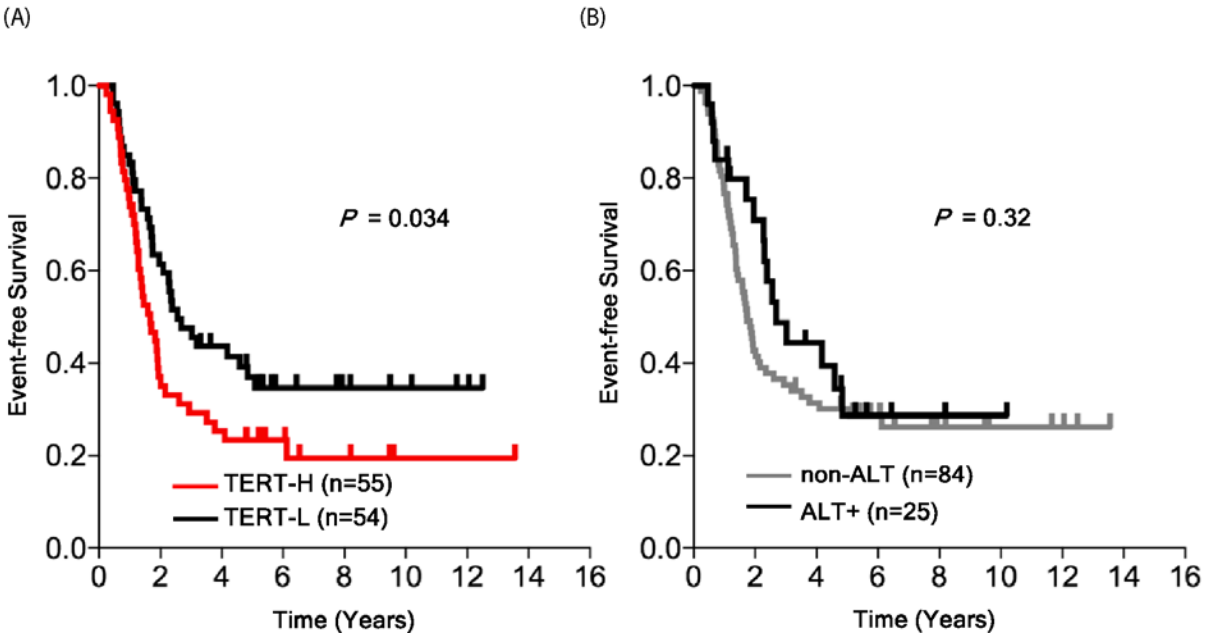

Fig. S10. Event-free survival in high-risk neuroblastoma patients based on TERT expression and ALT status. (A) Kaplan-Meier EFS curves in high-risk neuroblastoma patients (n=107) based on *TERT* expression. The patients are divided into *TERT*-high (TERT-H, n = 54; red) and *TERT*-low (TERT-L, n = 53; black) according to the median *TERT* mRNA expression. (B) Kaplan-Meier event-free survival curves in high-risk neuroblastoma patients (n=107) based on ALT status, ALT positive in black and non-ALT in grey. *P*-value was calculated using log-rank test.

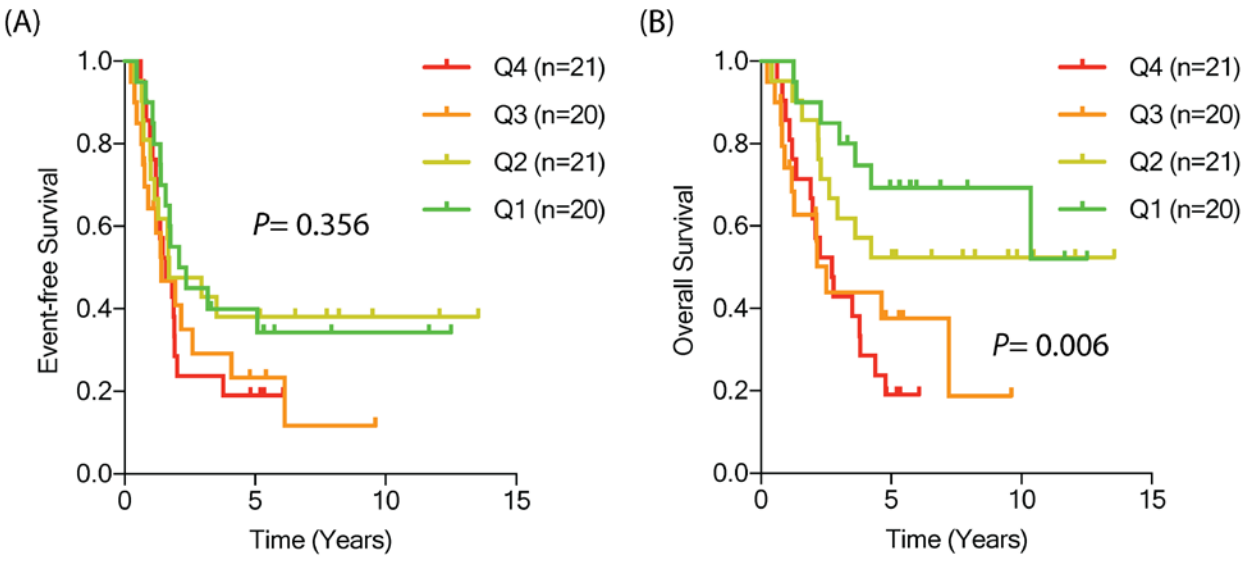

Fig. S11. EFS and OS in non-ALT high-risk neuroblastoma tumors based on *TERT* expression quartiles. (A) EFS and (B) OS based on *TERT* expression, grouped based on quartiles. *P*-value was calculated using the log-rank test

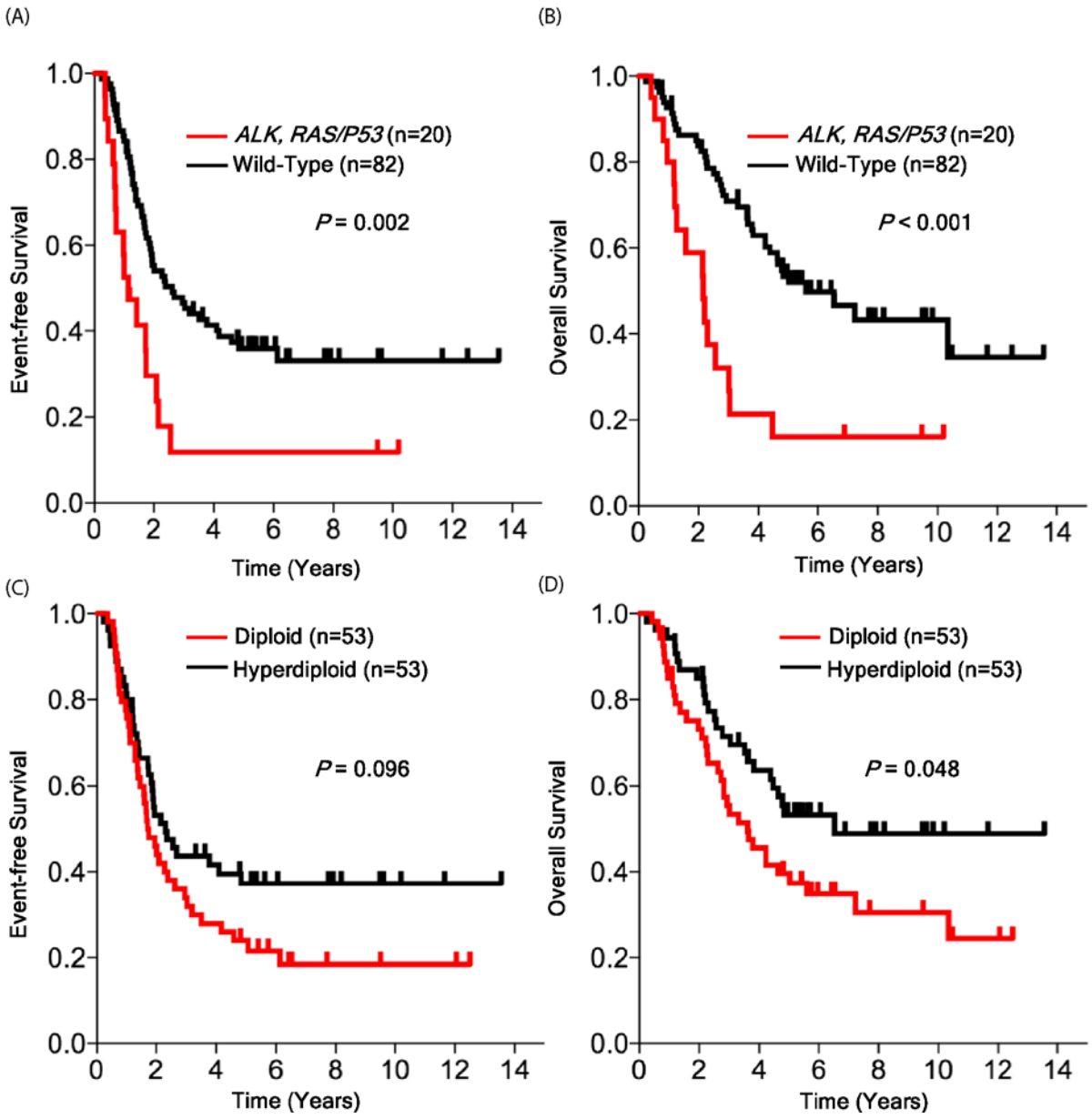

Fig. S12. *ALK, RAS/TP53* genomic alterations and ploidy are associated with poor outcomes in high-risk neuroblastoma. (A) EFS and (B) OS based on presence of ALK or RAS/p53-pathway genomic alterations in high-risk neuroblastoma patients. (C) EFS and (D) OS based on ploidy in high-risk neuroblastoma patients. *P*-value was calculated using the log-rank test

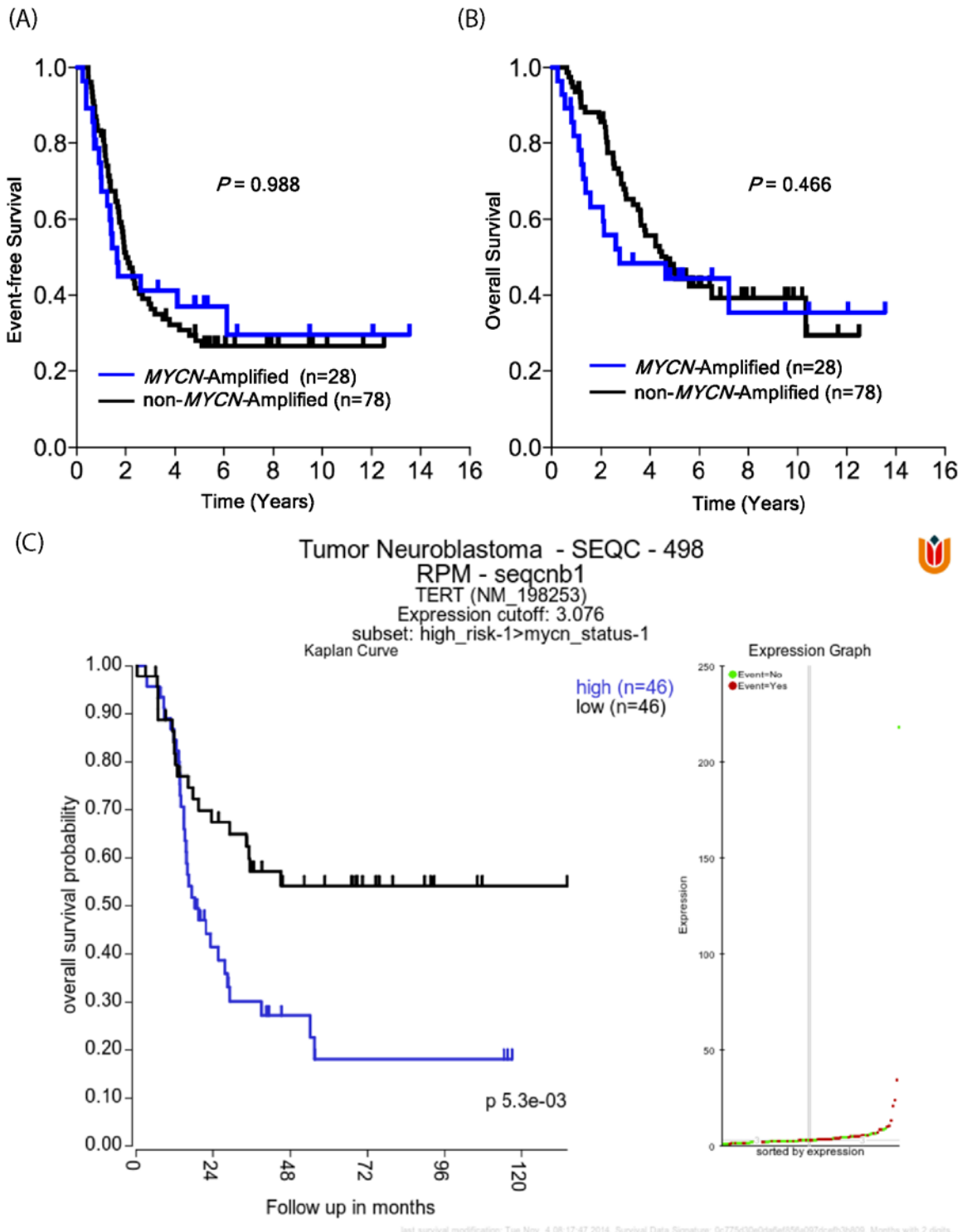

Fig. S13. Event-free survival and overall survival of patients based on *MYCN* amplification, and *TERT* expression in *MYCN*-amplified tumors. (A) Kaplan-Meier event-free survival, and (B) overall survival curves based on *MYCN*-amplification in high-risk neuroblastoma tumors. (C) Validation of results in Fig. 3F using the publicly available SEQC data set. Kaplan-Meier overall survival curves were constructed by segregating the *MYCN*-amplified subset based on

median *TERT* mRNA expression, median TERT expression was used for this analysis. *P*-value was calculated using the log-rank test.

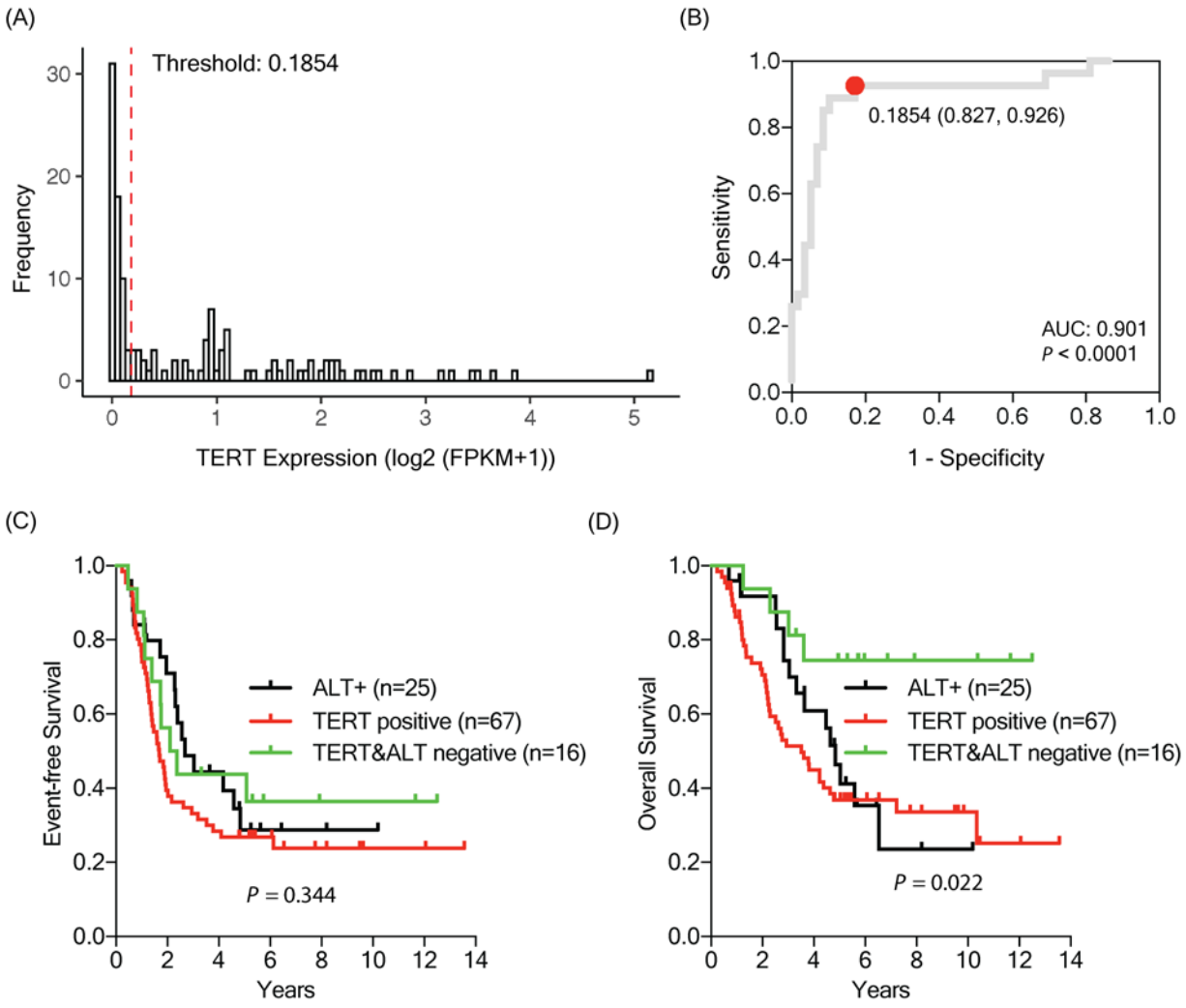

Fig. S14. Identification of TERT expression threshold. (A) Histogram for *TERT* expression (Log_2(FPKM+1)), in 134 neuroblastoma tumors with RNA sequencing. TERT expression threshold is shown as x intercept (red dashed line). (B) Receiver operating characteristic (ROC) curve analysis for *TERT* expression threshold in samples with WGS (n=85). TERT expression threshold determined in (A) is highlighted in red, specificity and sensitivity are mentioned in parentheses. ROC curve is constructed based on assumption that all *TERT* rearrangement tumors and *MYCN* amplified tumors are positive for *TERT* expression. (C) EFS and (D) OS for high-risk patients based on ALT status and TERT expression threshold. Patients are classified as ALT+ if their tumors are positive for C-circles irrespective of *TERT* expression, TERT positive if *TERT* expression is ≥ *TERT* threshold, and remaining patient tumors are classified as TERT&ALT negative. *P*-value was calculated using the log-rank test for survival curves**.**

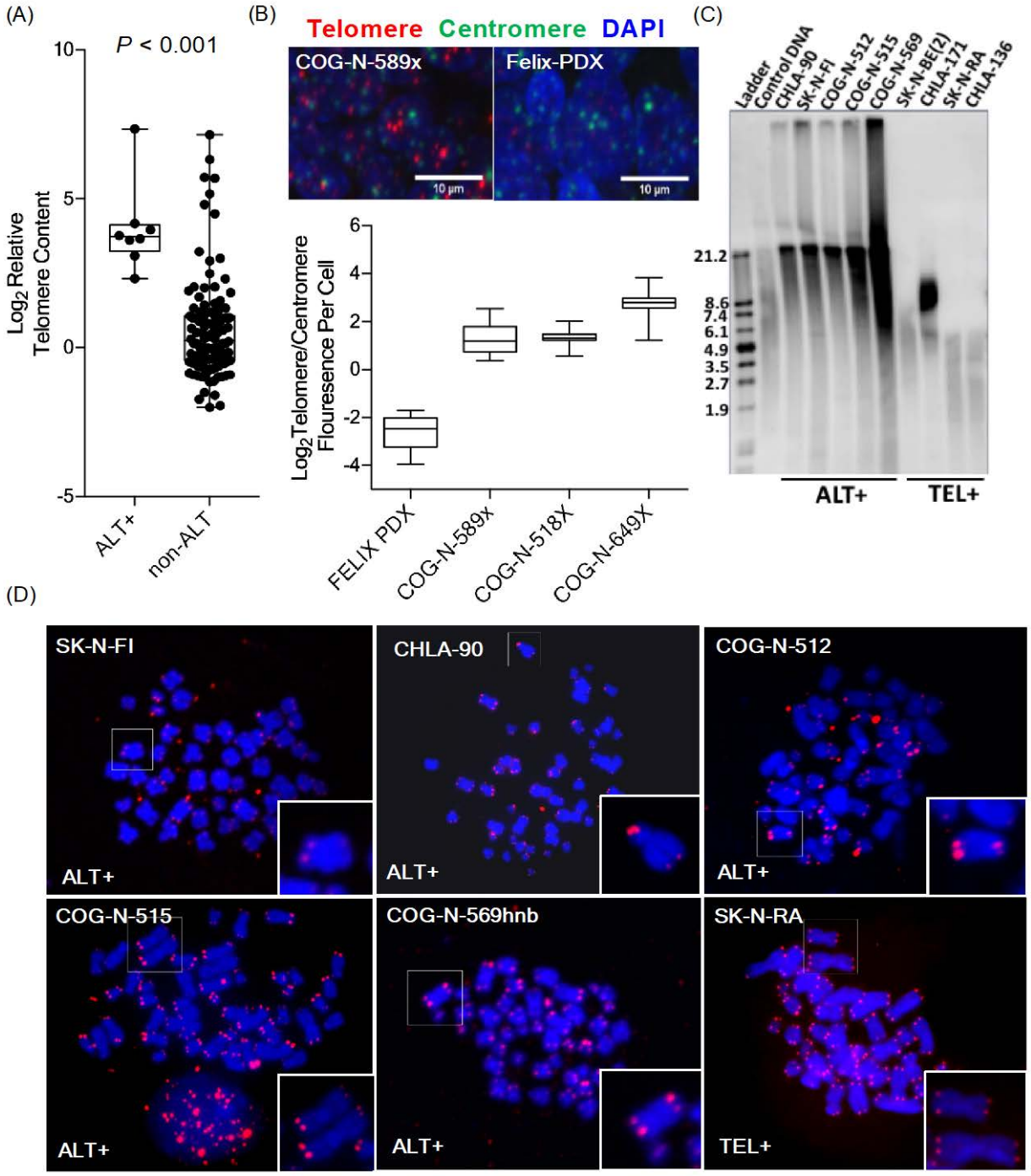

Fig. S15. ALT neuroblastoma cell lines and PDXs are associated with high telomere content. **(**A) Box plot showing relative telomere content in ALT versus non-ALT neuroblastoma cell lines and patient derived xenografts (B) Representative images of telomere (red) and centromere (green) FISH on an ALT PDX (COG-N-589X) and on a telomerase-positive PDX (Felix-PDX). (C) Box plot showing telomere/centromere fluorescence ratio in a telomerase-positive PDX (Felix-PDX) versus 3 ALT PDX models. (D) TRF blot showing high and heterogeneous telomere length in ALT neuroblastoma cell lines (CHLA-90, SK-N-FI, COG-N-512, COG-N-515 and COG-N-

569hnb) compared to telomerase-positive cell lines (SK-N-BE(2), CHLA-171, SK-N-RA, CHLA-136). (E) Telomere FISH on metaphase spreads in 5 ALT cell lines versus the telomerase positive cell line SK-N-RA. The magnified inset shows heterogeneous telomere signal (red) at chromosomal ends in the ALT cell lines.

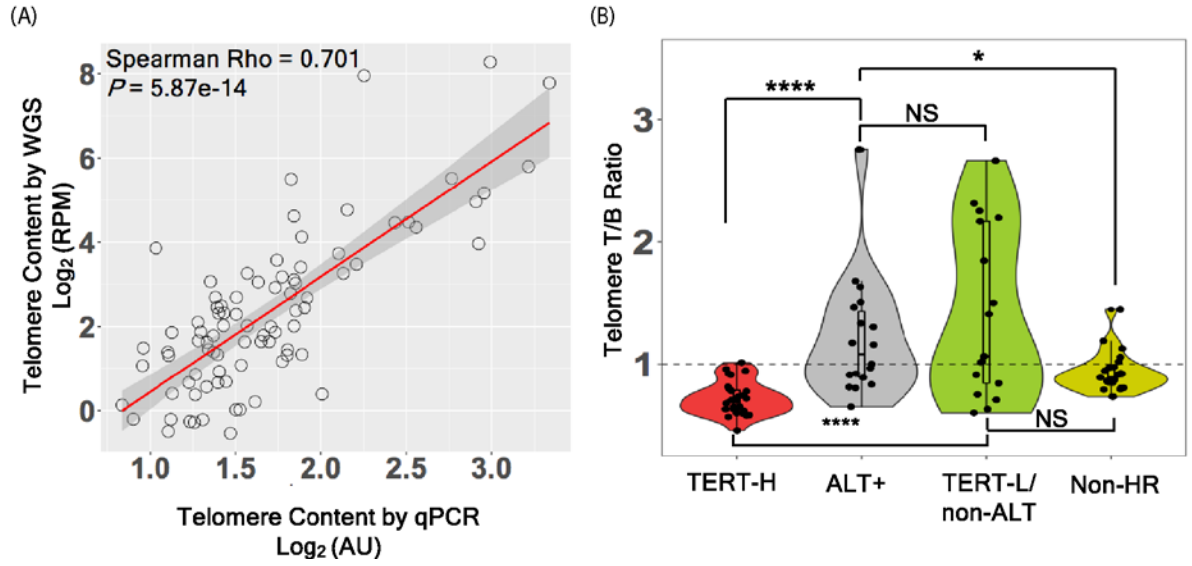

Fig. S16. Increased telomere abundance in ALT and TERT-L/non-ALT subgroups of high-risk neuroblastoma. (A) Correlation of telomere abundance measured by qPCR versus WGS data in 85 neuroblastoma tumor samples. Correlation was determined using spearman correlation test. (B) Violin plot represents distribution of WGS-based estimation of telomeric DNA abundance ratio between matched tumor and blood samples in TERT-H, ALT, TERT-L/non-ALT, and non-high-risk tumors. Y-intercept (dotted line) at T/B ratio 1 was added for reference. *: $P < 0.05$, ****: $P < 0.0001$. *P*-value was calculated using Wilcoxon sum rank test.

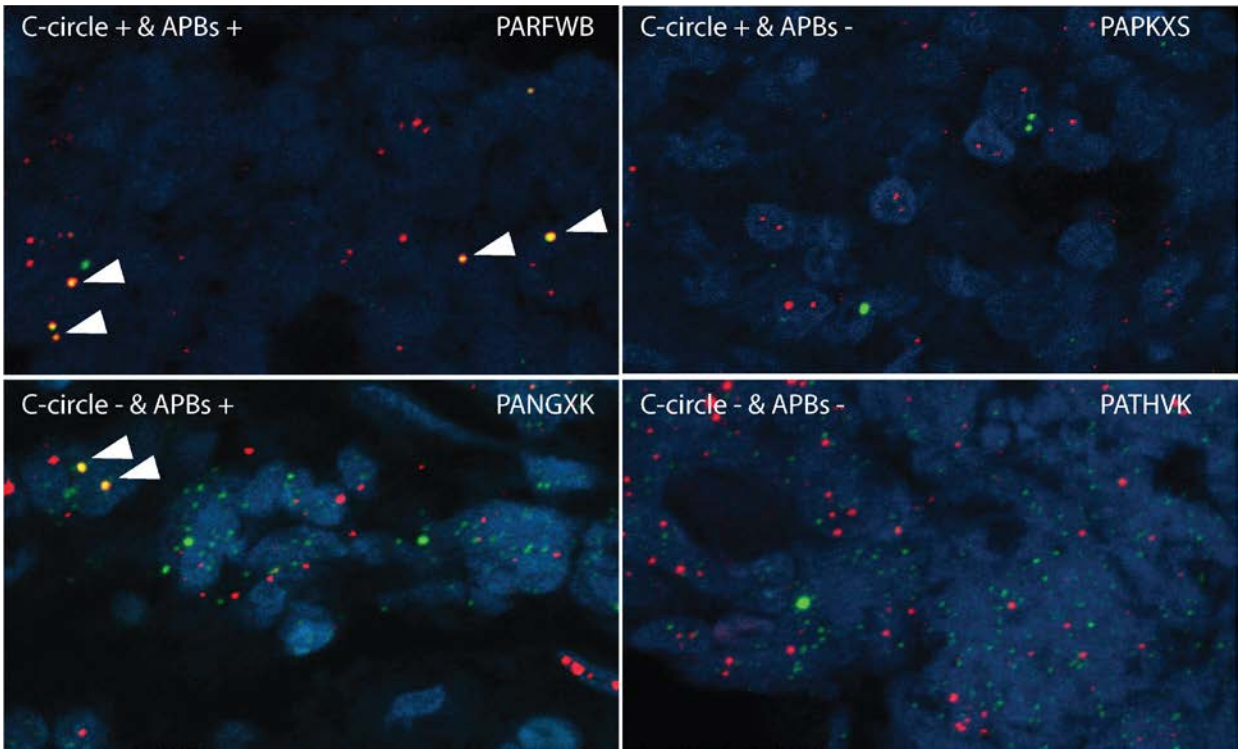

Fig. S17. Analysis of ALT associated promyelocytic leukemia bodies (APBs) in primary patient tumors. Representative IF-FISH images obtained for APB analysis in primary patient tumors. Images above represents 4 types of APB results observed in all the patient samples assessed for APBs. Telomeres were stained in green, PML bodies in red, and nuclei with DAPI (blue).

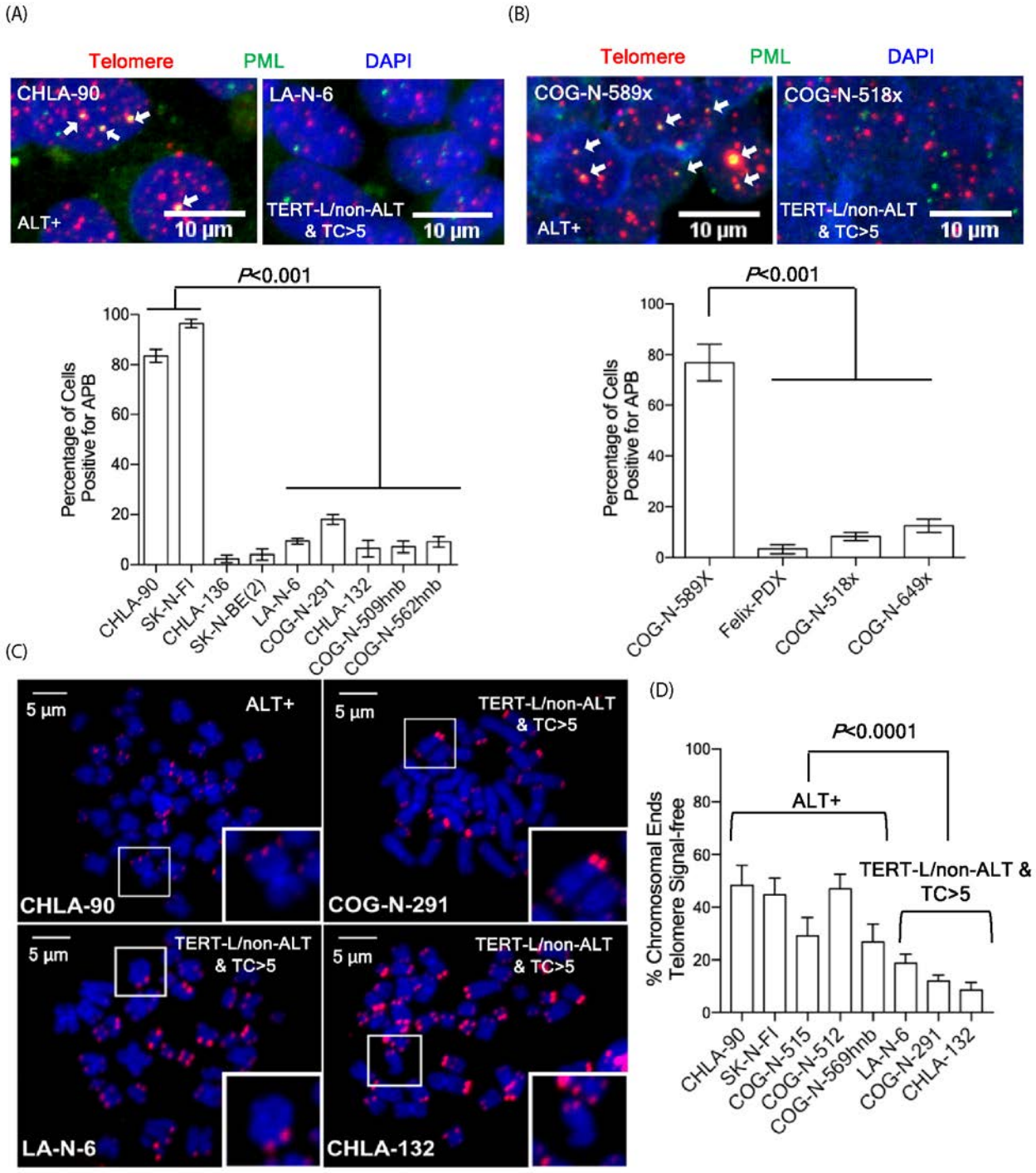

Fig. S18. TERT-L/non-ALT neuroblastoma cell lines and PDXs with high telomere content lack APBs and have fewer signal free chromosome ends than ALT cell lines. Representative images of APB analysis by IF-FISH (top panels) in (A) LA-N-6 versus ALT cell line (CHLA-90), and (B) in COG-N-518x versus ALT PDX (COG-N-589x). Telomeres stained red, PML bodies green, and nuclei with DAPI (blue). Bar graphs (A bottom panel) represent the percentage of APB-positive cells in LA-N-6, COG-N-291, CHLA-132, COG-N-509hnb, COG-N-562hnb

neuroblastoma cell lines compared to ALT (CHLA-90 and SK-N-FI) and telomerase positive (CHLA-136, SK-N-BE(2)) CLs. Bar graphs (b bottom panel) represents percentage of APB-positive cells in COG-N-518x, and COG-N-649x compared to ALT (COG-N-589x) and telomerase-positive (Felix-PDX) PDXs. (C) Telomere FISH on metaphase spreads in an ALT cell line (CHLA-90) and in LA-N-6, COG-N-291, and CHLA-132. The magnified inset shows heterogeneous telomere signal at chromosome ends. (D) Bar graph represents percentage of chromosomal ends that are signal-free in LA-N-6, COG-N-291, and CHLA-132 versus ALT cell lines (CHLA-90, SK-N-FI, COG-N-512, COG-N-515 and COG-N-569hnb).

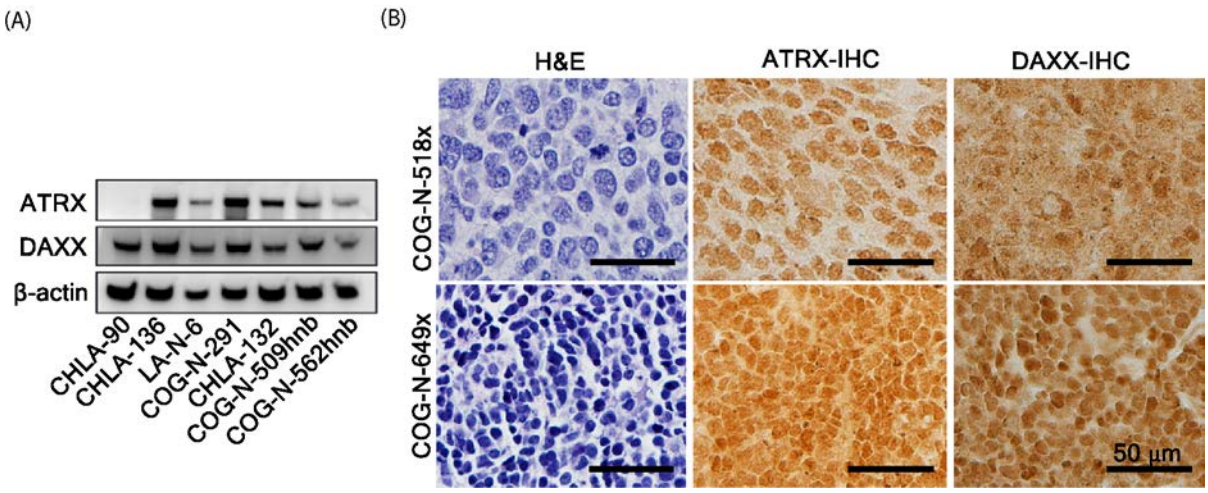

Fig. S19. TERT-L/non-ALT neuroblastoma CLs and PDXs with high telomere content express ATRX and DAXX protein. (A) Immunoblotting for ATRX, DAXX and β-actin in LA-N-6, COG-N-291, CHLA-132, COG-N-509hnb and COG-N-562hnb. ALT cell line (CHLA-90) with ATRX loss was used as a negative control. (B) H&E staining, ATRX IHC, and DAXX IHC in COG-N-518x, and COG-N-649x.

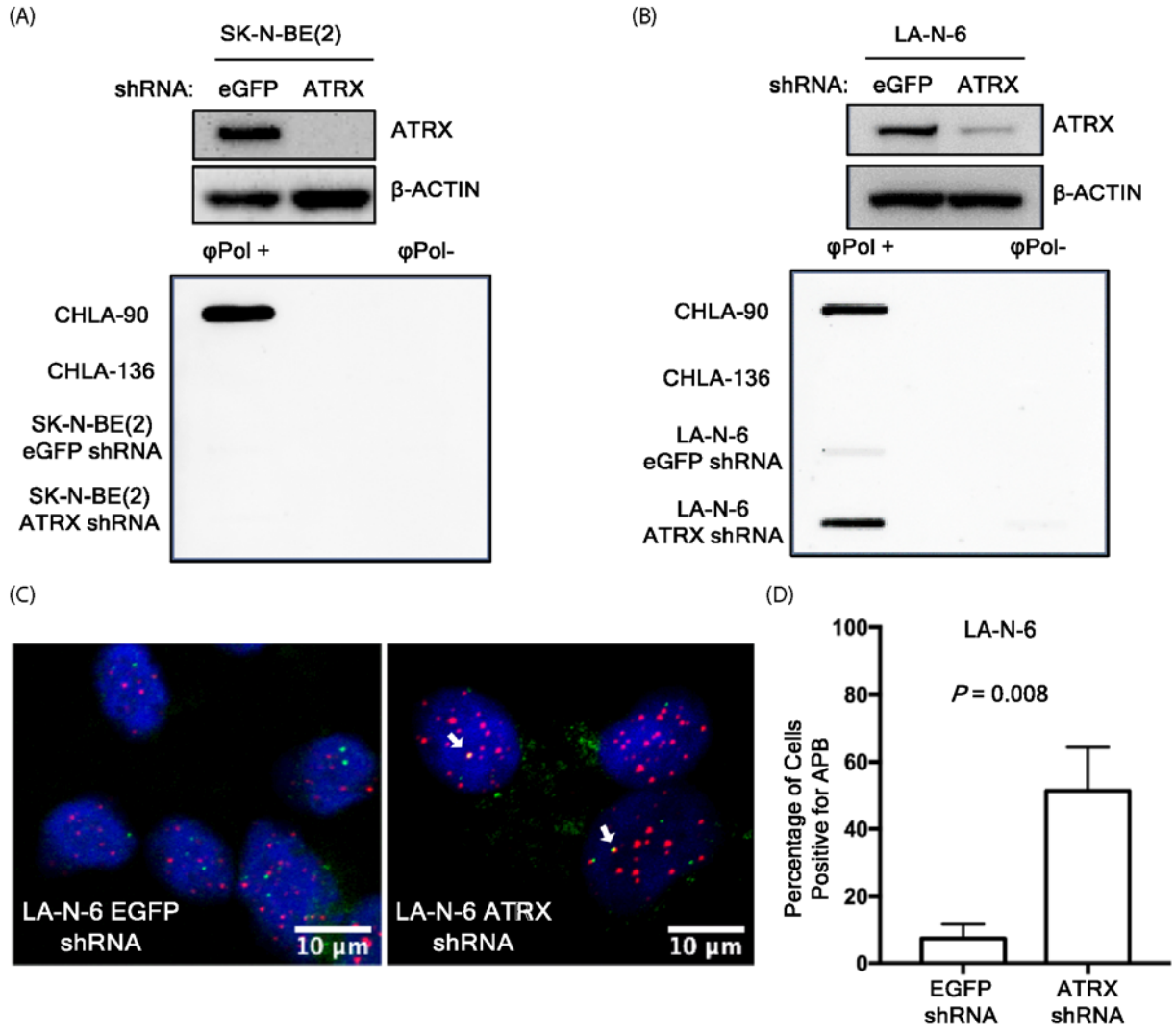

Fig. S20. ATRX knockdown is sufficient to induce the ALT phenotype in a TERT-L/non-ALT cell line but not in a telomerase-positive cell line. (A) Immunoblot for ATRX and β-actin following stable transduction with either eGFP shRNA or ATRX shRNA in telomerase-positive cell line (SK-N-BE(2)), and (B) in TERT-L/non-ALT cell line with high telomere content (LA-N-6). (A and B bottom panels) C-circle assay by slot blotting. The ALT cell line CHLA-90 was used as a positive control and telomerase-positive cell line CHLA-136 as negative control for the C-circle assay. (C) APB analysis in the same cells as B. (D) Bar graph shows the percentage of cells positive for APB staining in the same cells as B.

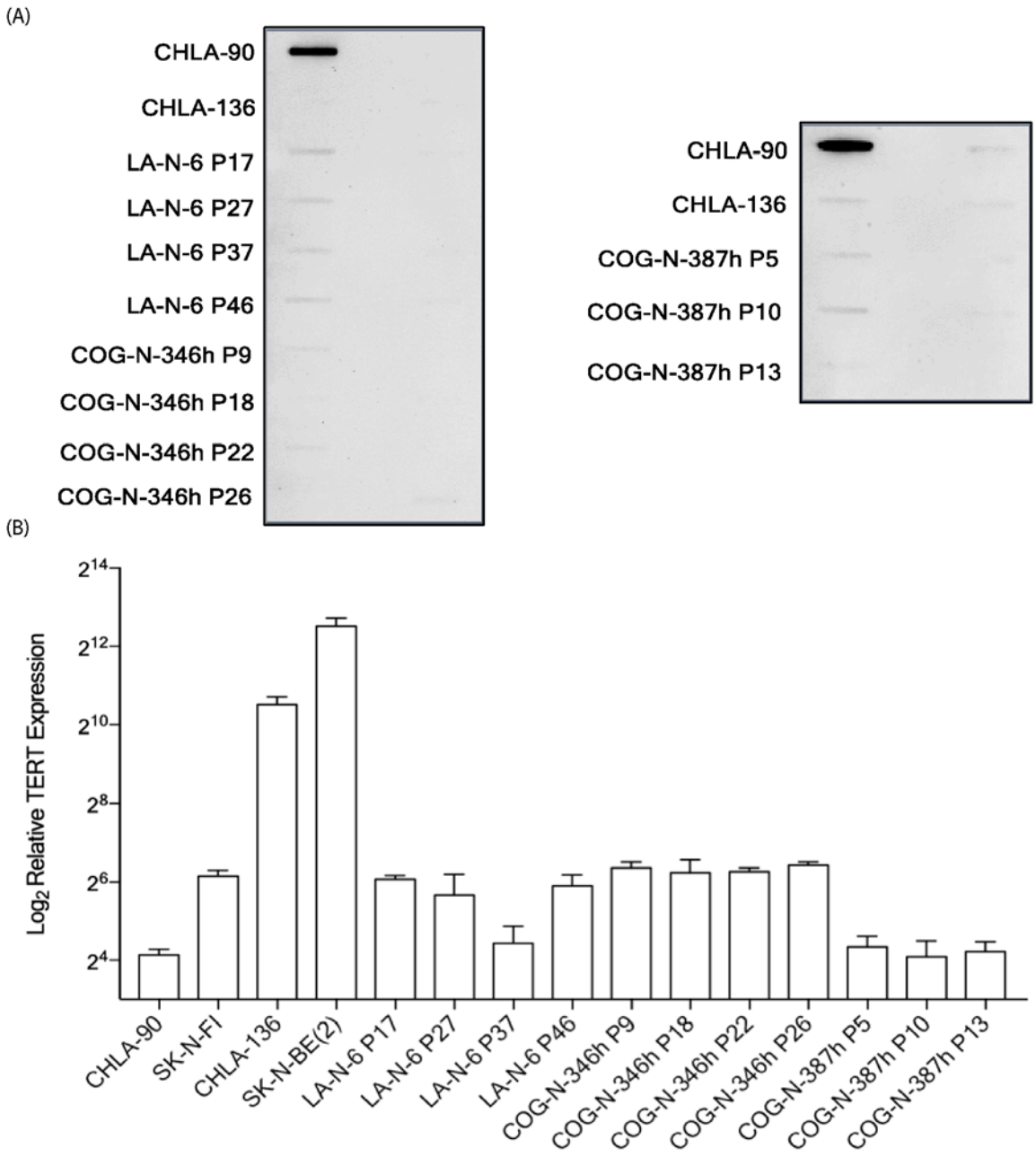

Fig. S21. ALT and telomerase-negative high-risk neuroblastoma cell lines remain negative for C-circles and *TERT* mRNA expression across multiple passages. (A) C-circle assay by slot blotting in telomerase-negative high-risk neuroblastoma cell lines across progressive passages in culture. (B) Relative *TERT* expression in the same cells as above. ALT cell lines (CHLA-90 and SK-N-FI) and telomerase-positive cell lines (CHLA-136 and SK-N-BE(2)) are used as controls.

Supplementary Tables

Table S1 (Excel). Table lists TARGET ID, data availability, C-circle positivity, *TERT* mRNA expression, *TERT.SV* positivity, telomere content, *MYCN* amplification, ALK alterations, p53/CDKN2A alterations, RAS pathway alterations and clinical data for primary patient tumors used in this study and 11 additional tumors studied that had altered *ATRX* (2nd tab).

Table S2 (Excel). Patient-derived neuroblastoma cell lines (1st tab) and PDXs (2nd tab) used in this study.

Table S3. Patient characteristics relative to ALT status in 134 neuroblastoma samples.

	ALT Positive (n=25)	ALT Negative (n=109)	*P*-value
Sex			
Male	13	69	*P*=NS
Female	12	40	
Age			
< 18 months	0	27	
≥ 18 months	25	82	*P*<0.001
Stage			
2-3 and 4s	0	25	
4	25	84	*P*<0.001
COG Risk Group			
High	25	85	*P*<0.001
Intermediate	0	12	
Low	0	12	
Ploidy			
Diploid	13	46	
Hyperdiploid	12	62	*P*=NS
Unknown	0	1	
***MYCN* Amplification**			
Amplified	0	30	
Non-Amplified	25	78	*P*<0.001
Unknown	0	1	
***ATRX* Staus**			
Genomic Alterations	15	0	*P*<0.001
Wild Type	10	102	
Unknown	0	7	

Supplementary References

1. Pugh TJ, Morozova O, Attiyeh EF, Asgharzadeh S, Wei JS, Auclair D, *et al.* The genetic landscape of high-risk neuroblastoma. *Nature genetics* **2013**;45:279-84.
2. Pertea M, Pertea GM, Antonescu CM, Chang TC, Mendell JT, Salzberg SL. StringTie enables improved reconstruction of a transcriptome from RNA-seq reads. *Nat Biotechnol* **2015**;33:290-5.
3. Heaphy CM, de Wilde RF, Jiao Y, Klein AP, Edil BH, Shi C, *et al.* Altered telomeres in tumors with ATRX and DAXX mutations. *Science (New York, NY)* **2011**;333:425.
4. Tomayko MM, Reynolds CP. Determination of subcutaneous tumor size in athymic (nude) mice. *Cancer Chemother Pharmacol* **1989**;24:148-54.
5. Makena MR, Koneru B, Nguyen TH, Kang MH, Reynolds CP. Reactive Oxygen Species-Mediated Synergism of Fenretinide and Romidepsin in Preclinical Models of T-cell Lymphoid Malignancies. *Mol Cancer Ther* **2017**;16:649-61.
6. Rokita JL, Rathi KS, Cardenas MF, Upton KA, Jayaseelan J, Cross KL, *et al.* Genomic Profiling of Childhood Tumor Patient-Derived Xenograft Models to Enable Rational Clinical Trial Design. *Cell Rep* **2019**;29:1675-89 e9.
7. Henson JD, Cao Y, Huschtscha LI, Chang AC, Au AY, Pickett HA, *et al.* DNA C-circles are specific and quantifiable markers of alternative-lengthening-of-telomeres activity. *Nat Biotechnol* **2009**;27:1181-5.
8. Henson JD, Reddel RR. Assaying and investigating Alternative Lengthening of Telomeres activity in human cells and cancers. *FEBS Lett* **2010**;584:3800-11.
9. Lau LM, Dagg RA, Henson JD, Au AY, Royds JA, Reddel RR. Detection of alternative lengthening of telomeres by telomere quantitative PCR. *Nucleic acids research* **2013**;41:e34.
10. Dagg RA, Pickett HA, Neumann AA, Napier CE, Henson JD, Teber ET, *et al.* Extensive Proliferation of Human Cancer Cells with Ever-Shorter Telomeres. *Cell Rep* **2017**;19:2544-56.
11. Flynn RL, Cox KE, Jeitany M, Wakimoto H, Bryll AR, Ganem NJ, *et al.* Alternative lengthening of telomeres renders cancer cells hypersensitive to ATR inhibitors. *Science* **2015**;347:273-7.
12. Drmanac R, Sparks AB, Callow MJ, Halpern AL, Burns NL, Kermani BG, *et al.* Human genome sequencing using unchained base reads on self-assembling DNA nanoarrays. *Science (New York, NY)* **2010**;327:78-81.
13. Cesare AJ, Heaphy CM, O'Sullivan RJ. Visualization of Telomere Integrity and Function In Vitro and In Vivo Using Immunofluorescence Techniques. *Curr Protoc Cytom* **2015**;73:12 40 1-31.
14. Henson JD, Hannay JA, McCarthy SW, Royds JA, Yeager TR, Robinson RA, *et al.* A robust assay for alternative lengthening of telomeres in tumors shows the significance of alternative lengthening of telomeres in sarcomas and astrocytomas. *Clin Cancer Res* **2005**;11:217-25.
15. Venturini L, Motta R, Gronchi A, Daidone M, Zaffaroni N. Prognostic relevance of ALT-associated markers in liposarcoma: a comparative analysis. *BMC Cancer* **2010**;10:254.

16. Farooqi AS, Dagg RA, Choi LM, Shay JW, Reynolds CP, Lau LM. Alternative lengthening of telomeres in neuroblastoma cell lines is associated with a lack of MYCN genomic amplification and with p53 pathway aberrations. *J Neurooncol* **2014**;119:17-26.